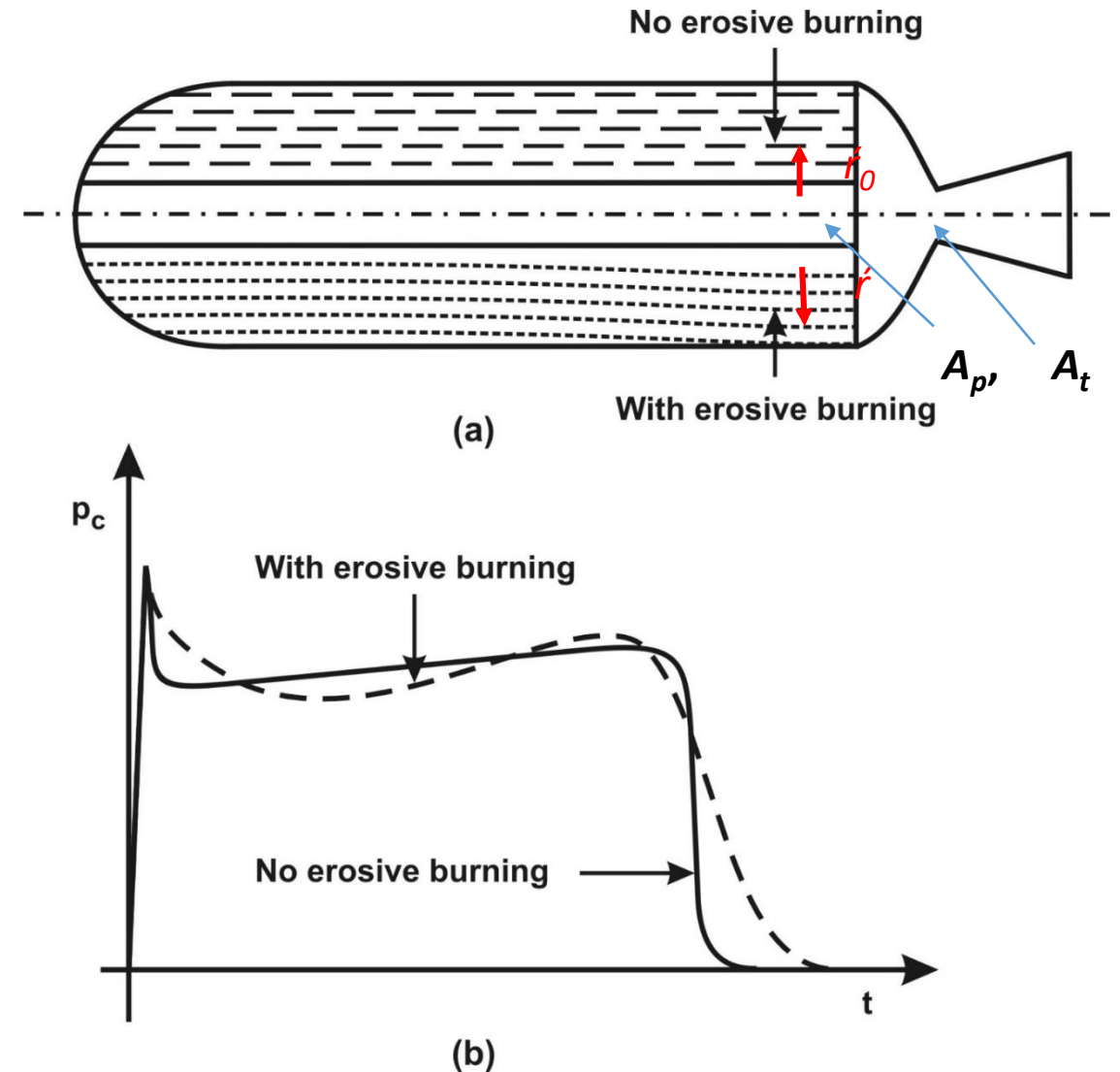


Vignettes from insights into the Erosive burning in solid propellants

- What is erosive burning?
- Historical - 1958, 1960, 1977-78, 1979, 1981 - 1986, 1997-1998, 2004, 2014, 2018
- Experimentalists of significance: Marklund and Lake, 1960; Ishihara and Kubota, 1986
Other experimentalists: Kenneth Kuo, King, Razdan, Murphy
- Crucial confusions of the mid eighties due to the principal actors -
Kenneth Kuo, Beddini, Merril King, Leon Strand, Cohen
- Misses and the hits - HSM, PJP

What is erosive burning?

- Solid propellant Burn rate, \dot{r} depends on propellant composition, pressure, initial Temperature and lateral velocity of gases
- The dependence on pressure and initial temperature is set out as \dot{r}_0
- The ratio $\eta = \dot{r} / \dot{r}_0$ is called erosive burning ratio and is dependent on the lateral velocity of gases.
- The pressure time curve in a rocket motor is influenced by erosive burning.
- As the gas velocity increases through the port, the mass flux also increases, reduces the boundary layer thickness so enhancing the heat transfer into the propellant grain.
- Static pressure decreases with increase in the mass flux that partly contributing to the reduction in the non-erosive burn rate.
- The usual parameter characterizing it is $J = A_t/A_p$



Further,

- It is simple to see that if \mathcal{J} is large, erosive burning effects will be significant.
- One standard recommendation is to keep \mathcal{J} low so that erosive effects are marginal (the usual choice is <0.5).
- ISRO rocket motors belong to this category.

- But tactical rocket motors (defense applications) that are volume limited need high solid loading. This naturally increases \mathcal{J} .
- Thus tactical rocket motor design must include erosive burning behavior in propellant grain design.
- The incremental effects of erosive burning have been studied using many different techniques by experimenters.....

King's Apparatus

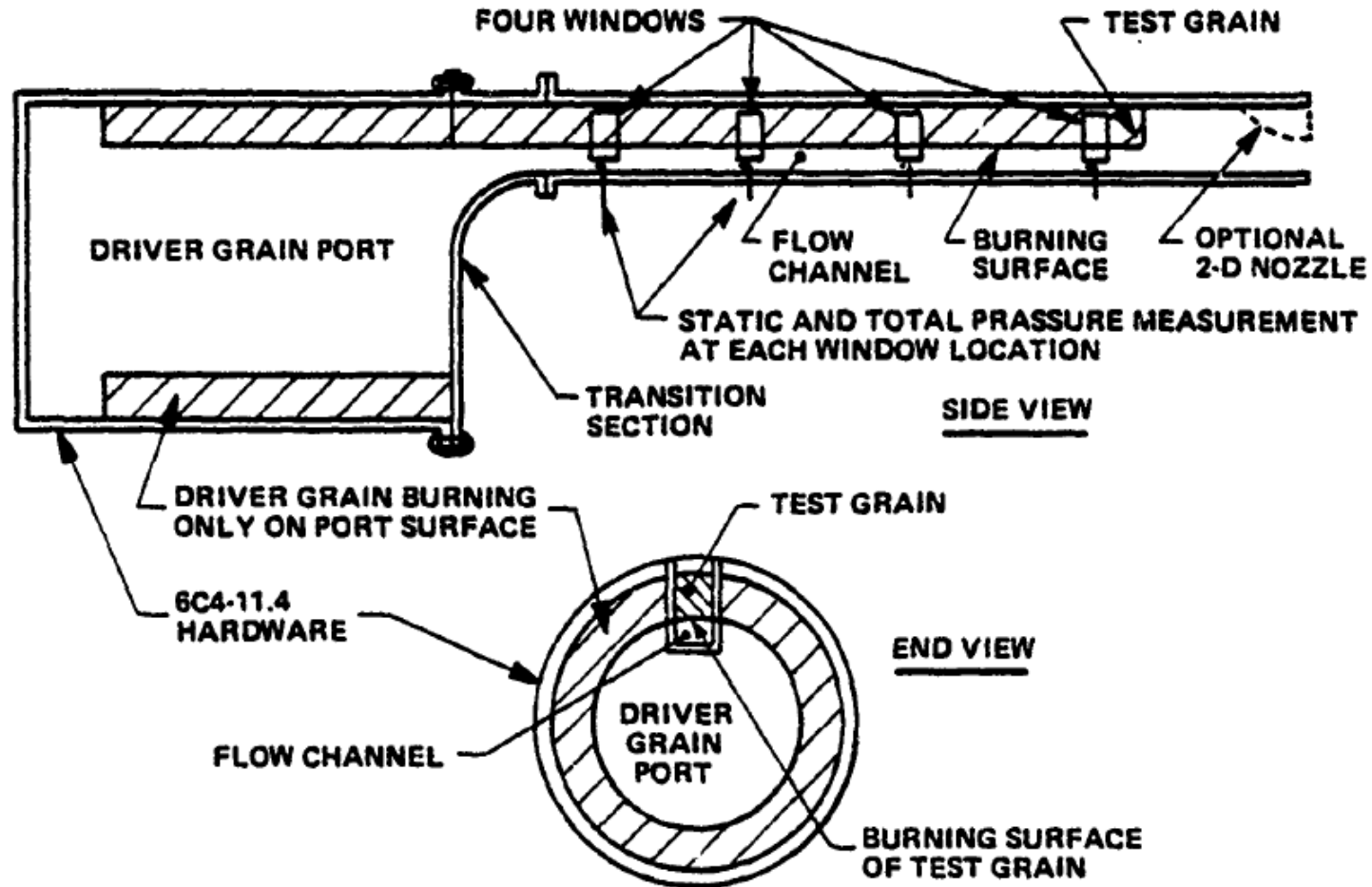


Figure 3. Schematic Drawing of Erosive Burning Test Apparatus.

Razdan and Kuo's facility

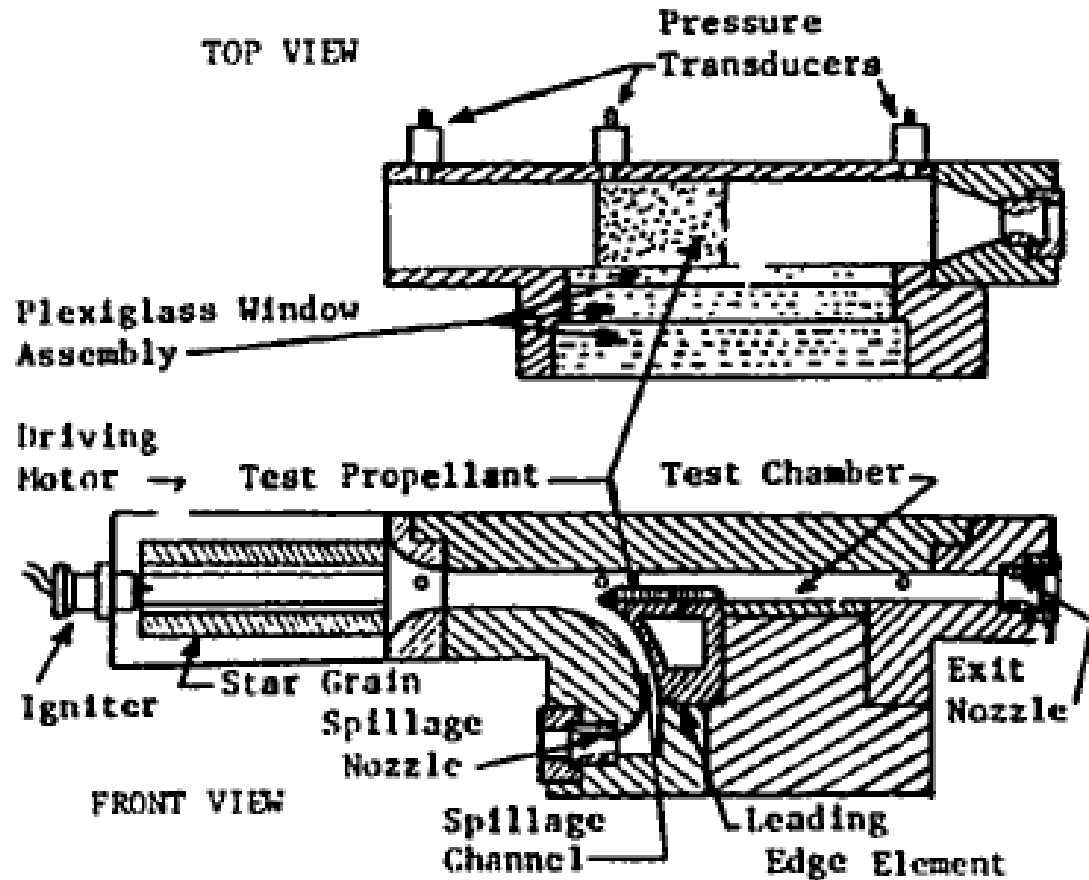


Fig. 1 Schematic diagram of erosive burning test rig.

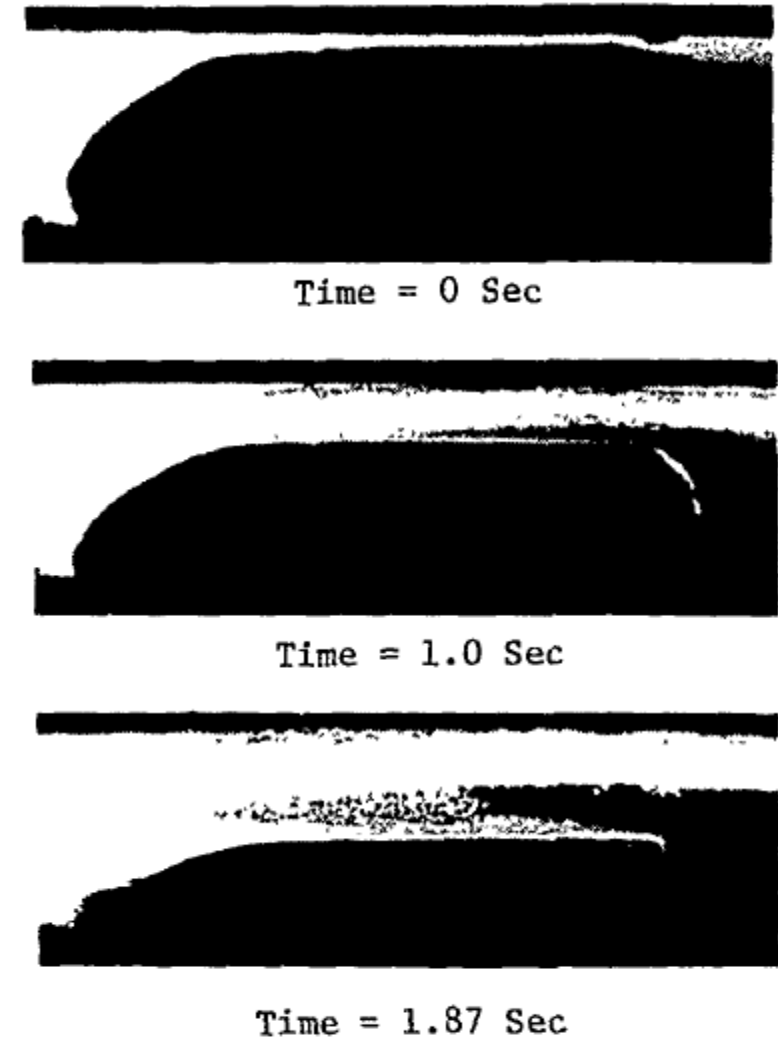


Fig. 4 Photographs showing location of test-propellant surface at various times during a test firing.

Typical data from Razdan and Kuo

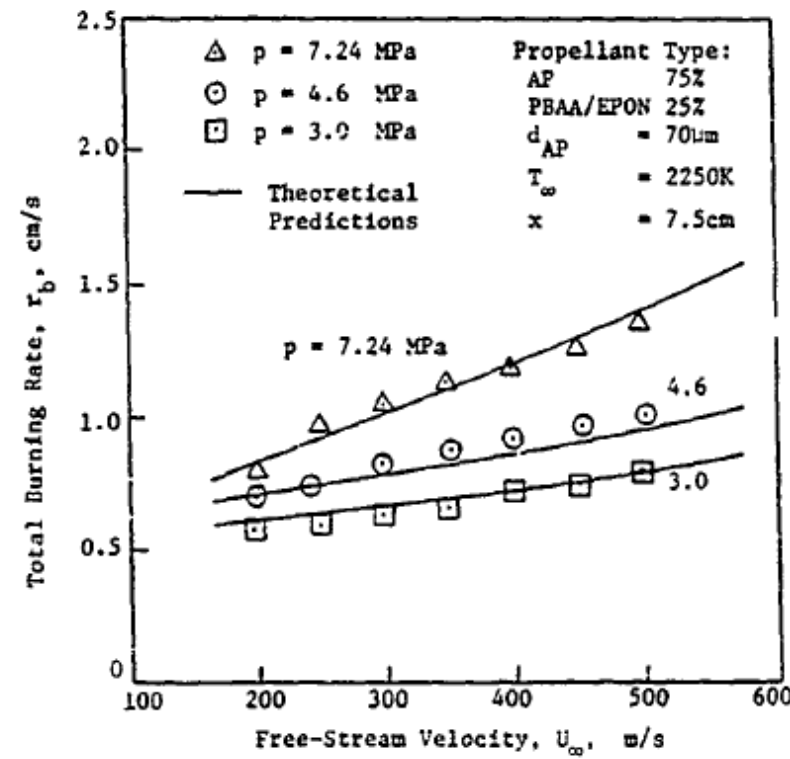


Fig. 7 Comparison of predicted burning rates with experimental data at various pressures and freestream velocities for propellant III.

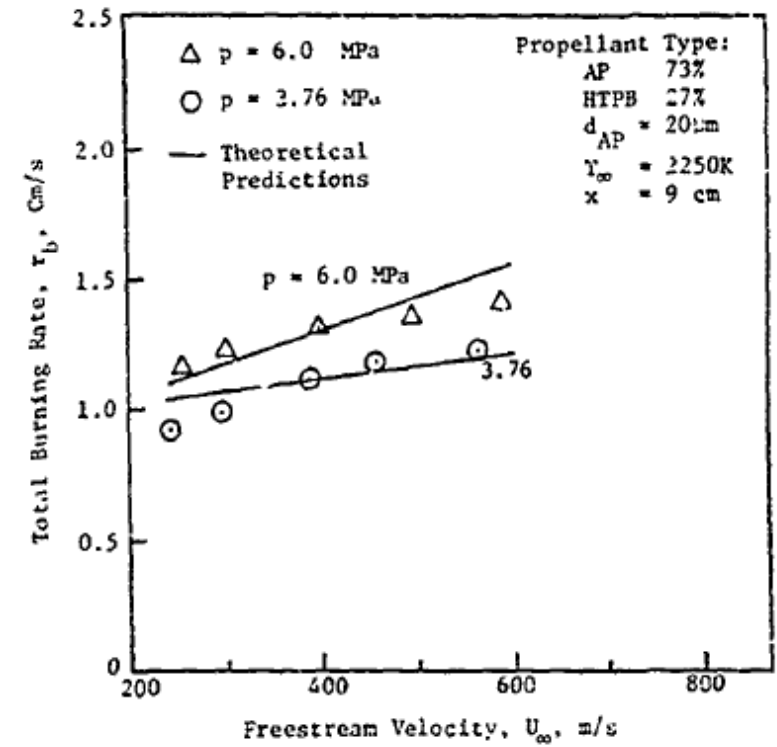


Fig. 8 Comparison of predicted burning rates with experimental data at various pressures and freestream velocities for propellant I.

M. K. RAZDAN AND K. K. KUO


Table 1 Propellant data

Propellant type	I (4525)	II (5051)	III
Composition	AP/HTPB	AP/HTPB	AP/PBAA-EPON
Average particle size, μm	20	200	76
Weight percent of oxidizer	73	73	75
Pre-exponent a in the strand burning rate law, $(\text{cm/s}) (\text{MPa})^{-n}$	0.305	0.2026	0.2452
Pressure exponent n in the strand burning rate law	0.5611	0.5427	0.41
Flame temperature of propellant gas, K	1667	1667	1920
Propellant density, kg/m^3	1492	1492	1600

From Razdan and Kuo, AIAA J, p. 669, 1980

C. Erosive-Burning Rate Correlations

Using the measured experimental data, correlations were developed between erosive burning rate augmentation factor (r_b/r_{b0}), freestream velocity, and pressure. The functional form of these correlations was obtained from the experimental data, as explained in the following. The burning rate at a particular pressure is seen to increase somewhat linearly with freestream velocity. An equation relating burning rate and velocity can be written as


$$r_b = r_{b0} + \alpha (U_\infty - U_{th})^{n_u} \quad (4)$$

where U_{th} represents the threshold velocity and α is a constant which must be a function of pressure, since the experimental data indicate that the slope of the r_b vs U_∞ data changes with pressure. Therefore, the following relationship is assumed:


$$\alpha = \alpha_1 p^\omega \quad (5)$$

In this equation α_1 and ω are unknown constants. Although Eq. (4) contains the threshold velocity consideration, our experimental data for all three propellants tested showed no threshold effect. The threshold velocity is retained in Eq. (4) to maintain the generality of the form of the correlation.

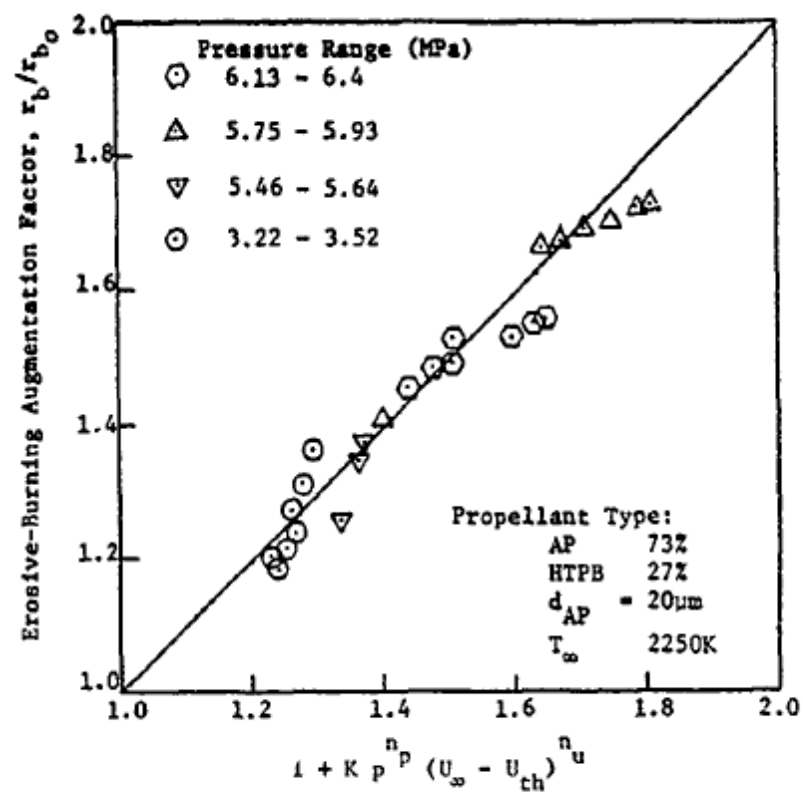


Fig. 11 Experimental data for erosive burning augmentation factor correlated with pressure and freestream velocity for propellant I.

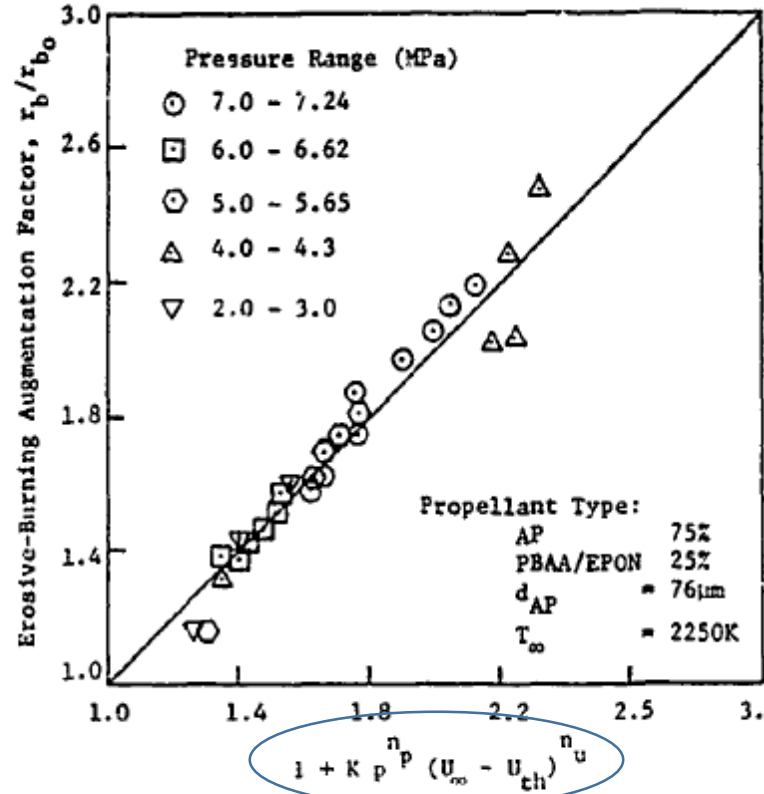


Fig. 13 Experimental data for erosive burning augmentation factor correlated with pressure and freestream velocity for propellant III.

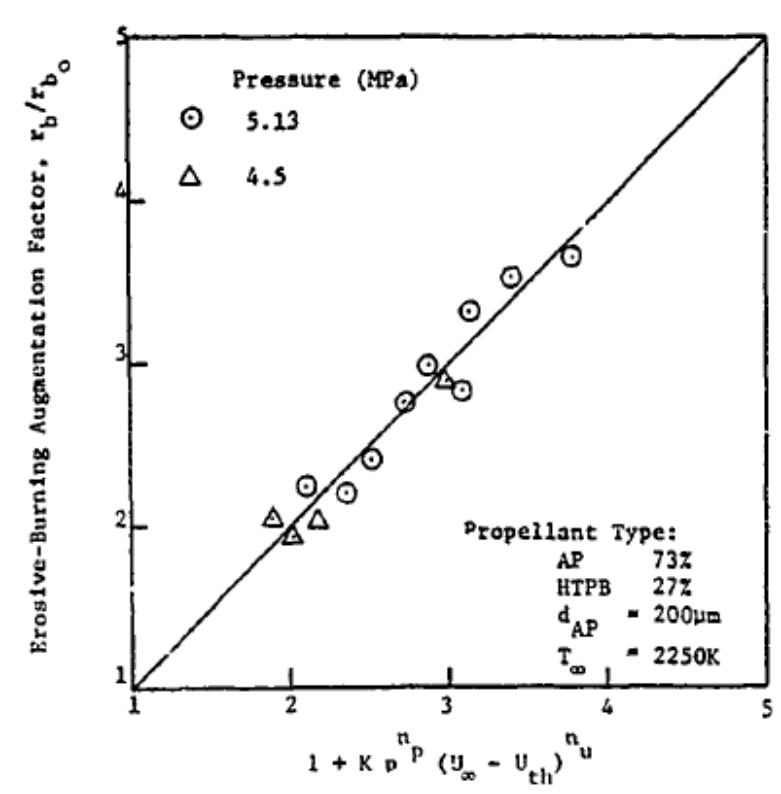


Fig. 12 Experimental data for erosive burning augmentation factor correlated with pressure and freestream velocity for propellant II.

Table 2 Correlation coefficients

Propellant type	I	II	III
$K, (\text{MPa})^{-n_p} (\text{m/s})^{-n_u}$	4.8×10^{-3}	3.167×10^{-4}	2×10^{-4}
n_p	0.35	1.463	0.705
n_u	0.69	1.42	1.252

These equations set out in 1981 - 83 have 3 constants while the earlier work of Lenoir and Robillard (1957) had only 2 constants!

Summary of experimental data

Propellants for which Erosive Burning Data are Available

Code	Propellant Composition	ρ_p (kg/m ³)	T_{ad} (K)	d_0 (mm)
Ishihara and Kubota [14]				
High energy	55.6NC + 40.4NG + 4.0DEP	1600	2716	20.0
Reference	50.4NC + 36.6NG + 13.0DEP	1600	2114	
Low energy	47.5NC + 34.5NG + 18.0DEP	1600	1778	
Marklund and Lake [15]				
Prop A	65AP (24–30 μm) + 35polyester	1620	1690	5.0
Prop C	75AP (24–30 μm) + 25polysulfide	1700	2550	
Lawrence et al. [5]				
Prop 1	68AP + 16Al + 16UTREZ	1700	—	12.5
Prop 2	84AP + 16UTREZ	1700	—	
Prop 3	68AP + 16Al + 16(PBAN + Fe ₂ O ₃)	1700	—	
Prop 4	68AP + 16Al + 16PBAN	1700	—	
Prop 5	72AP + 14Al + 16(CTPB + Fe _c 2O ₃)	1720	—	
Prop 6	73AP + 10Al + 17CTPB	1680	—	
Nagaoka et al. [6]				
	65AP + 16Al + 19PB	1550	—	20–90

.....More experimental data

King [25]

4525	73AP (20 μm) + 27HTPB	1500	1667	19
5051	73AP (200 μm) + 27HTPB	1500	1667	
4685	73AP (5 μm) + 27HTPB	1500	1667	
4869	72AP (20 μm) + 25HTPB + 2Fe ₂ O ₃	1500	1660	
5542	77AP (20 μm) + 27HTPB	1550	2065	
5565	68.4 (200 μm) + 13.6 (90 μm) AP + 18HTPB	1650	2575	
5555	41 (1 μm) + 41 (7 μm) AP + 18 HTPB	1650	2575	
6626	70 (90 μm) + 4 (200 μm) AP + 21 HTPB + 5Al	1600	2575	

Razdan and Kuo [9]

4525	73AP (20 μm) + 27HTPB	1500	1667	15
5051	73AP (200 μm) + 27HTPB	1500	1667	
	76AP (76 μm) + 24(PBAA + EPON)	1500	1920	

Godon et al. [17]

	80AP + 20CTPB	1590	2313	3-5
--	---------------	------	------	-----

Strand et al. [24]

	70AP + 14PBAN + 16Al	1770	3200	52, 102
--	----------------------	------	------	---------

Traineau and Keuntzmann [18]

	70AP + 14PBAN + 16Al	1770	3200	20
--	----------------------	------	------	----

Osborn et al. [19]

	65AP + 18CTPB + 17Al	1790	3100	
--	----------------------	------	------	--

EROSIVE AUGMENTATION OF SOLID PROPELLANT BURNING RATE:
MOTOR SIZE SCALING EFFECT*

40271

L. D. Strand
Jet Propulsion Laboratory, California Institute of Technology
Pasadena, California

P-13

and

N. S. Cohen
Cohen Professional Services
Redlands, California

ABSTRACT

Two different independent variable forms, a difference form and ratio form, were investigated for correlating the normalized magnitude of the measured erosive burning rate augmentation above the threshold, r/r_0 , in terms of the amount that the driving parameter (mass flux or Reynolds No.) exceeds the threshold value for erosive augmentation at the test condition. The latter was calculated from the previously determined threshold correlation. Either variable form provided a correlation for each of the two motor size data bases individually. However, the data showed a motor size effect, supporting the general observation that the magnitude of erosive burning rate augmentation is reduced for larger rocket motors. For both independent variable forms, the required motor size scaling was attained by including the motor port radius raised to a power in the independent parameter. A boundary layer theory analysis confirmed the experimental finding, but showed that the magnitude of the scale effect is itself dependent upon scale, tending to diminish with increasing motor size.

Lenoir & Robillard Theory

$$r = ap^n + \frac{\alpha G^{0.8}}{L^{0.2}} \exp\left(\frac{-\beta \rho_p r}{G}\right),$$

The present
non-dimensional
expression

$$\eta = 1 + K_1 (g^{0.8} - g_{th}^{0.8}) H (g - g_{th})$$

with

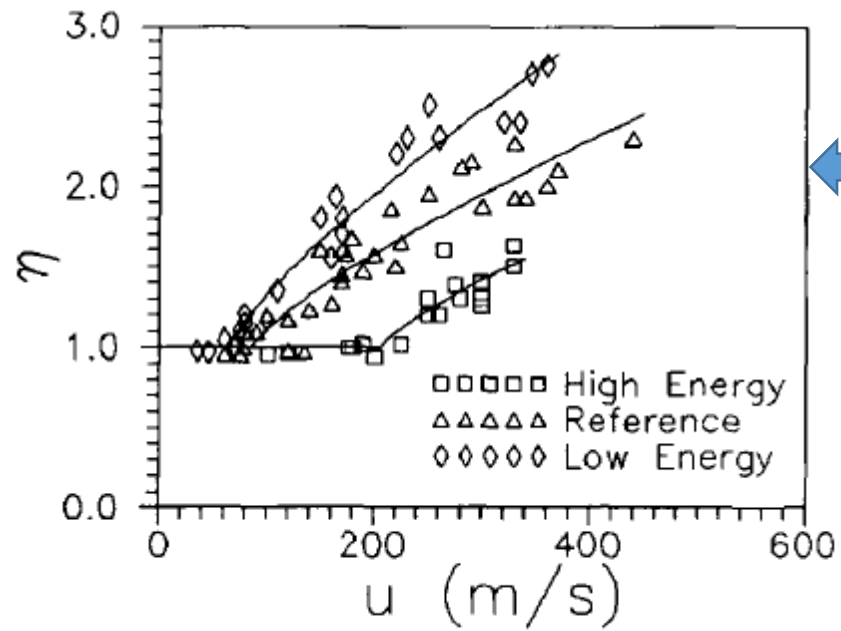
$$g = K_2 g_0 \text{Re}_0^m, \quad \eta = r / ap^n$$

$$\eta = 1 + 0.023 (g^{0.8} - g_{th}^{0.8}) H (g - g_{th}), \quad (12)$$

where $g = g_0 (\text{Re}_0 / 1000)^{-0.125}$ and $g_{th} = 35.0$.

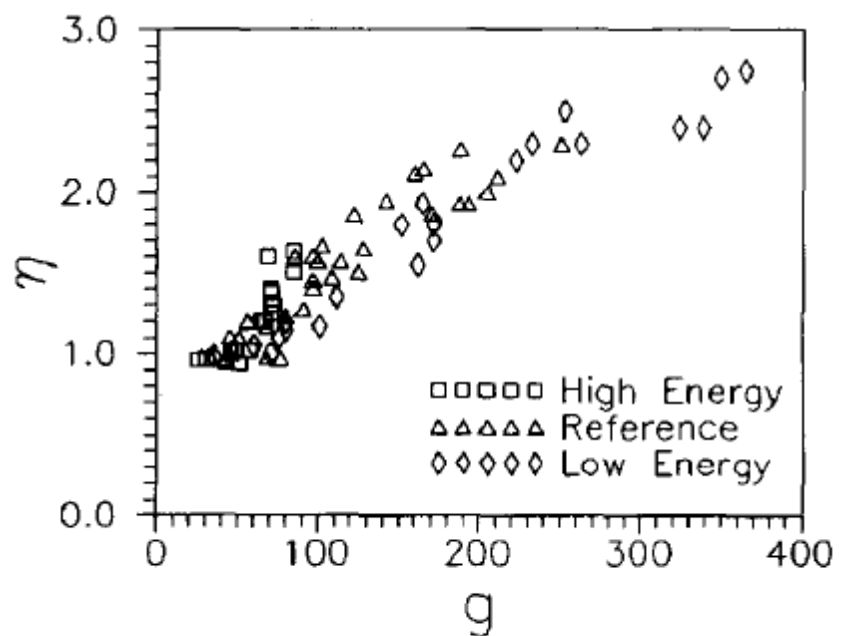
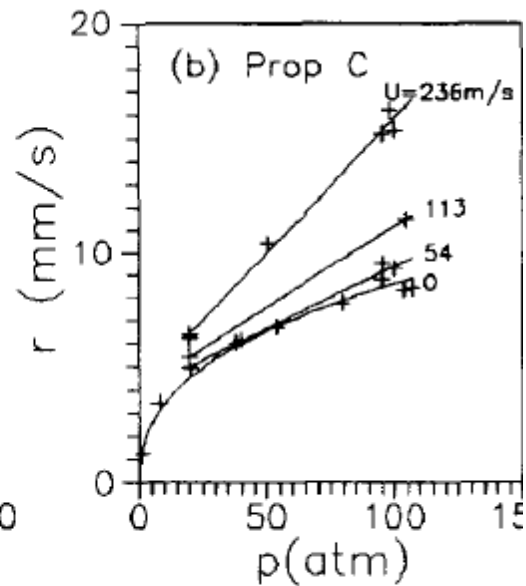
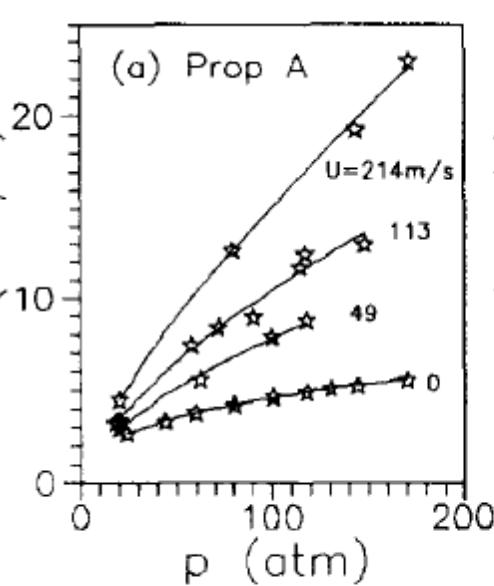
Re_0 Reynolds number based on propellant burn rate ($\rho_p r_0 d_0 / \mu$)

d_0 = port diameter, for partly symmetric geometries, is it hydraulic mean diameter = $4Ap/P$ or P/π ? To be seen later



Raw data from Ishihara and Kubota

And from Marklund and Lake



Data set against the dimensionless variable, g

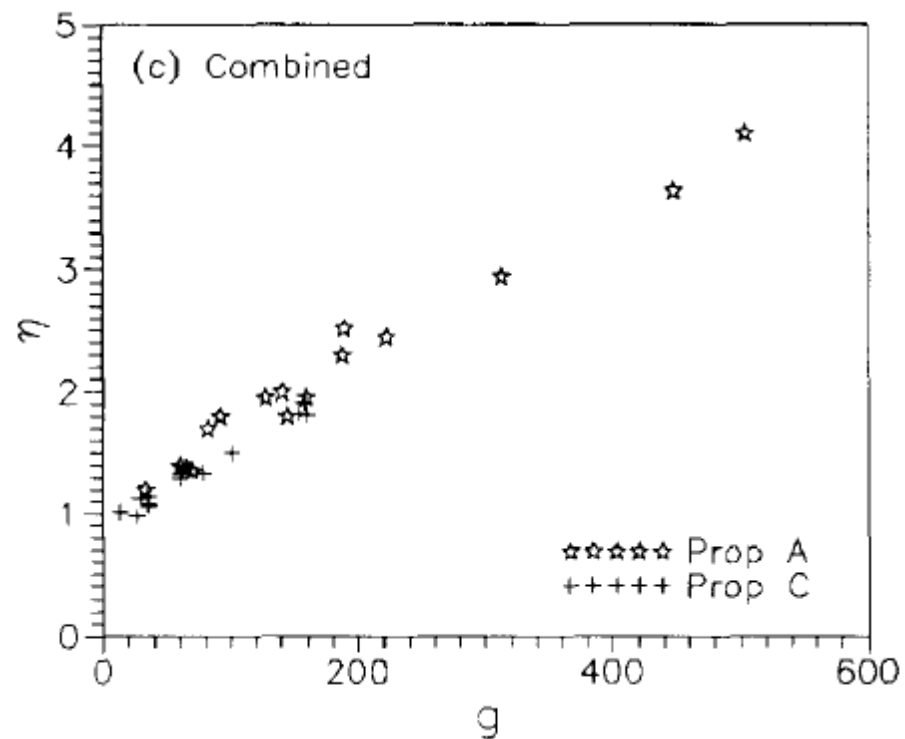


Fig. 1. Data of Ishihara and Kubota [14] (a) in terms of η vs u (m/s) and (b) in terms of η vs g (present work).

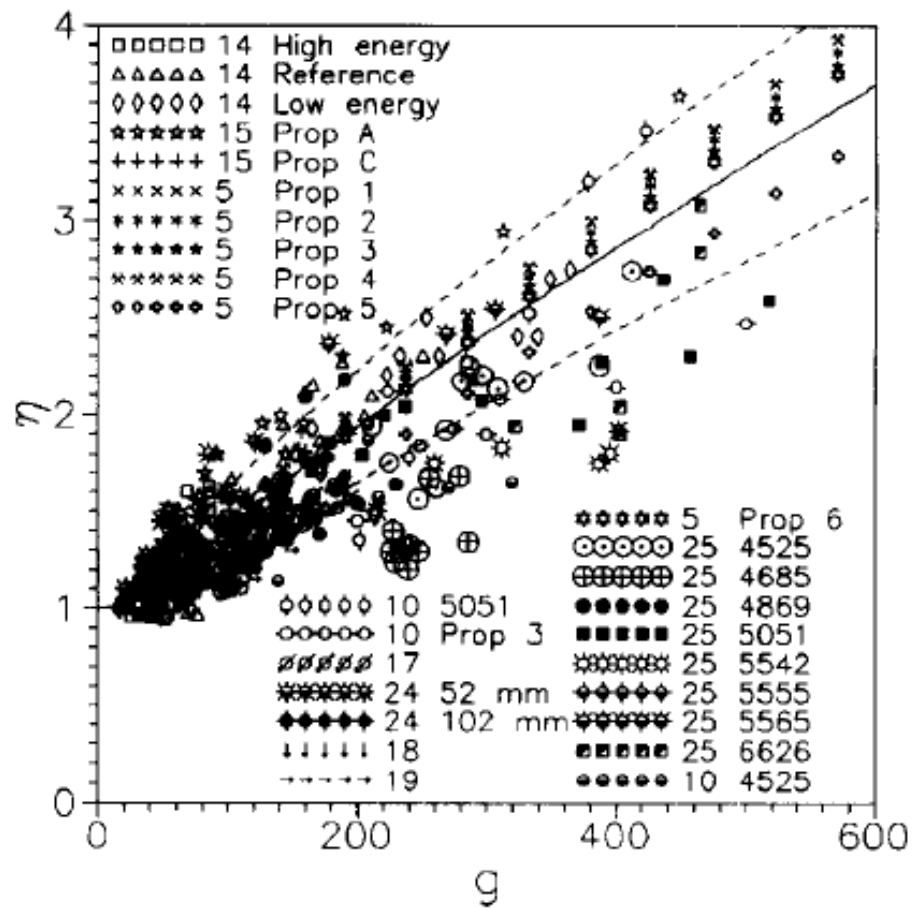


Fig. 9. Plot of η vs g for data of all authors for both double-base and composite propellants.

Many aspects of scatter in the data are due to the difficulty in extracting the erosive component from the experiments. The same propellant studied by two investigators has shown significant differences.

A new criterion $g < 35$ was set out for determining if erosive burning is significant

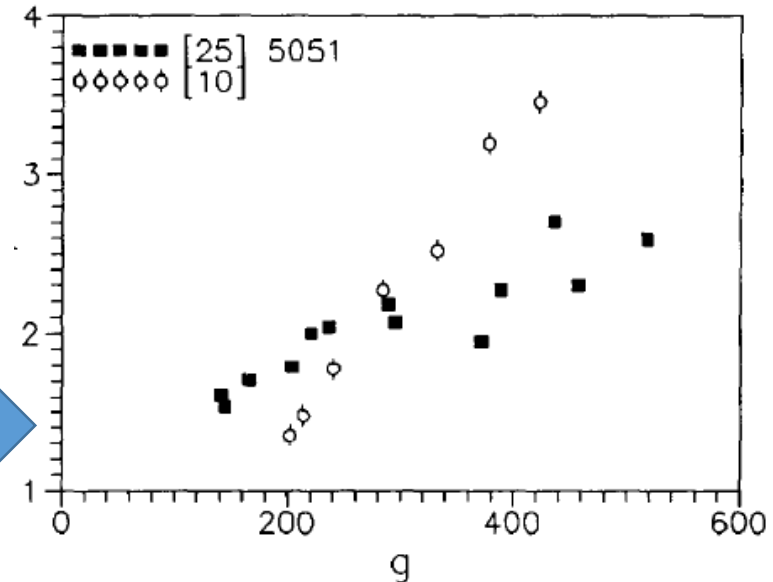
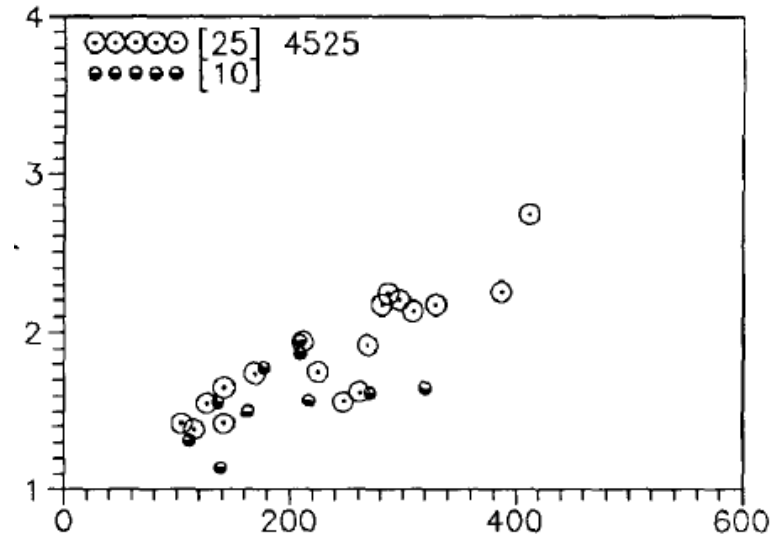


Fig. 7. Comparison of data from King [25, 26] and Razdan and Kuo [10] for propellants 4525 (a) and 5051 (b). The legend indicates reference number and propellant identification.

Then in 2000,

The erosive burning law got integrated into tactical rocket design in DRDL. One might think the matter has ended...pleasantly.....Not so soon!

Some time in 2011, it was brought out that the erosive burning law was not always giving good predictions (in comparison with experimental data) It turned out that this was consistently happening for non-axisymmetric grains - like the Fin-o-cyl grain they were dealing with then. This led to an investigation of the flow behavior through partially symmetric shapes.

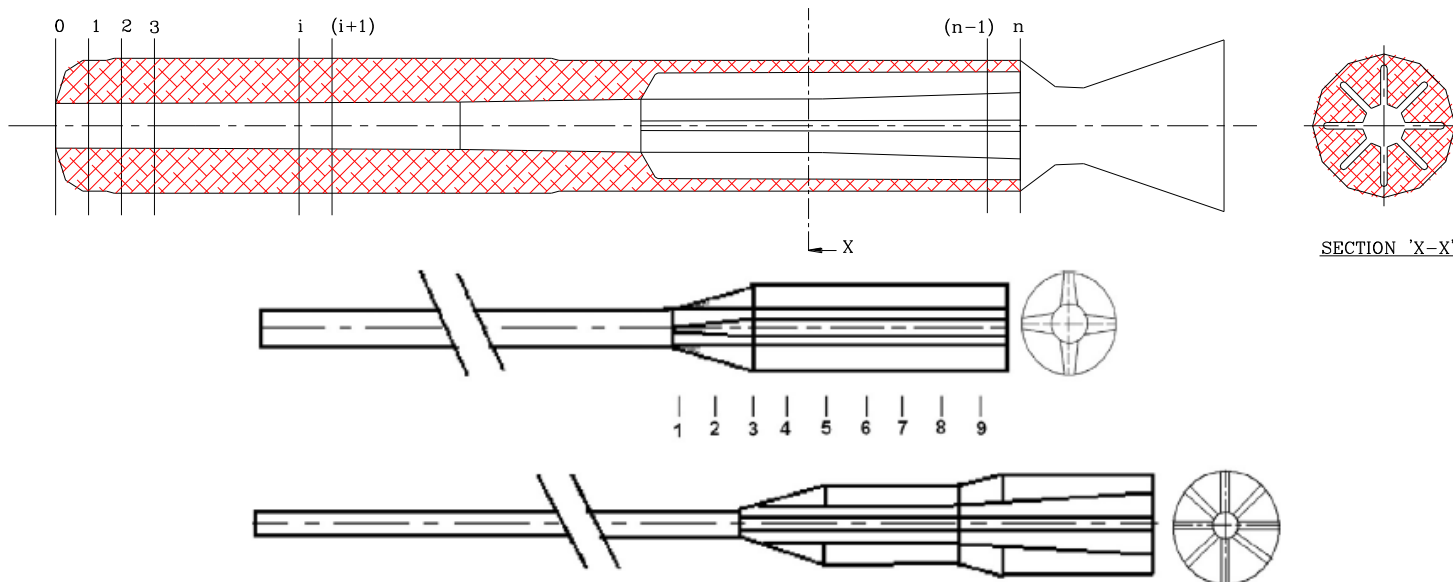


Fig. 1. Geometries of the two grains for Motor-1 (top) and Motor-2 (bottom); the first part is cylindrical and the aft part is finocyl with a transition region, the cross section shown on the right is of the aft end.

To explore the issues, CFD was applied for determining the flow distribution through the part symmetric geometry.....

Table 1

Properties of the motors under study.

Parameter	Motor-1	Motor-2
Motor length, m	2.1	4.8
Port diameter, m	0.17	Varies from 0.31 to 0.49
Initial cylindrical segment, m	1.37	3.48
Finocyl transition zone, m	0.18	0.26
Number of webs in the finocyl	4	8
Finocyl minimum dia., m	0.08	0.13
Finocyl maximum dia., m	0.17	Varies from 0.28 to 0.37
Throat diameter, mm	45	176
Burn rate at 7 MPa and pressure index, n	6.5 mm/s and 0.25	19 mm/s and 0.38

Extension of the universal erosive burning law to partly symmetric propellant grain geometries

H.S. Mukunda^a, P.J. Paul^a, Afroz Javed^b, Debasis Chakraborty^{b,*}

^a Indian Institute of Science, Bangalore, Karnataka, India

^b Defense Research and Development Laboratory, Hyderabad, Andhra Pradesh 500058, India

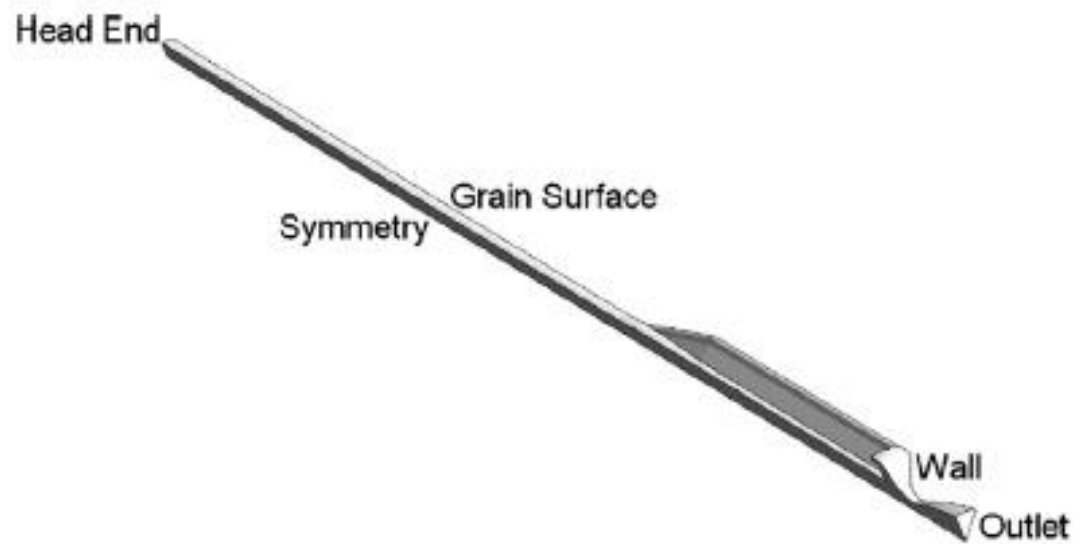


Fig. 2. Geometry of motor-1 for the simulation with the boundary locations.

Tetrahedral grids are made using ICEM CFD [7] package, a layer of hexahedral grids are used at walls and grain surface to resolve gradients. Three different grids of 0.74, 1.42, and 3.29 millions sizes with minimum normal grid spacing of 0.4, 0.1 and 0.01 mm are studied to establish the grid independence of the results. A typical grid is shown in Fig. 3. It can be observed that the grids near the geometrical changes are sufficiently clustered to capture high flow gradients expected in these regions. Minimum y^+ varies from head end to nozzle end and typical y^+ at head end and nozzle is of the order of 0.1 and 20, respectively.

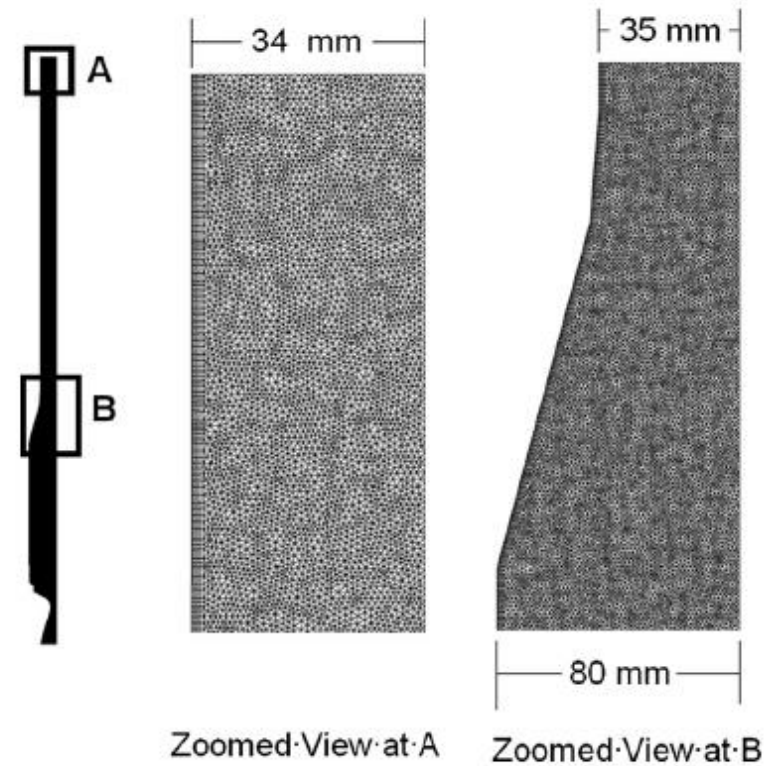


Fig. 3. Computational grid for the motor geometry.

The flow simulation is carried out using CFX11 commercial CFD solver [8]. It solves 3-D Navier-Stokes equations with $k-\epsilon$ turbulence model. For the present simulations, the grain surface is set as isothermal wall at 2980 K temperature and the propellant mass flow from the grain is considered as the source term in the mass continuity equation. Two sides are taken as symmetry boundary conditions and the nozzle wall and head end wall are taken as no slip adiabatic walls. Supersonic outflow boundary condition is prescribed at the outlet as the flow at the nozzle exit is supersonic.

A second order numerical scheme is utilized for the simulations. A physical time step of 0.2 ms is used for the steady state simulations. The simulation is run till a convergence level of 1×10^{-4} is reached on normalized logarithmic residuals.

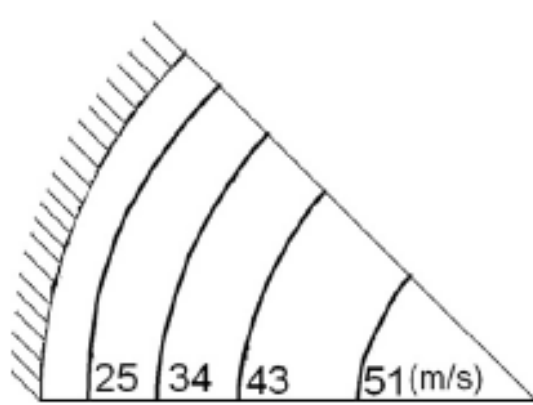


Fig. 4. The cross section of the propellant showing that at this section 0.44 m from the head end, the port is circular. Velocities are shown in on the contour lines. For instance contour line near the surface has a velocity of 25 m/s and contour close to the central region of the port has a velocity of 51 m/s.

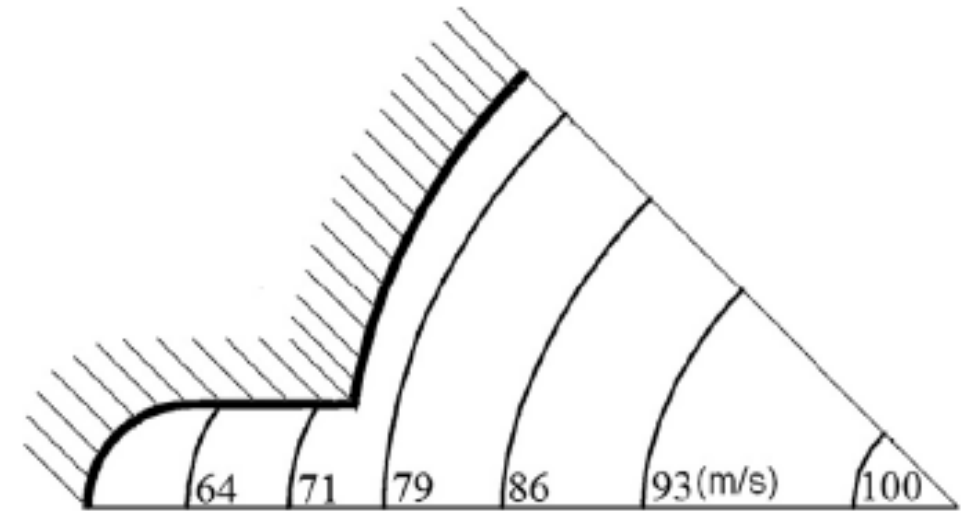


Fig. 5. The cross section of the propellant showing that at this section 1.43 m from the head end, the port is in transition to finocyl geometry.

Table 2
Geometrical properties and mass flow rates from different cross sections.

Sl. no.	Axial location (m)	Perimeter (m)	Port area $\times 10^3$ (m ²)	Mass flow rate (kg/s)	Mass flux (kg/m ² s)
1	1.37	0.24	4.49	3.20	710
2	1.43	0.35	5.33	3.41	640
3	1.53	0.52	7.53	3.89	520
4	1.63	0.54	7.84	4.48	570
5	1.73	0.54	7.88	5.05	640
6	1.82	0.54	7.92	5.60	710
7	1.91	0.55	7.96	6.15	770
8	2.01	0.55	8.01	6.76	840
9	2.08	0.55	8.04	7.14	890

Note that the mass flux over the central region is very much more than in the outer regions. Erosive burning is sensitive to the flux near the surface

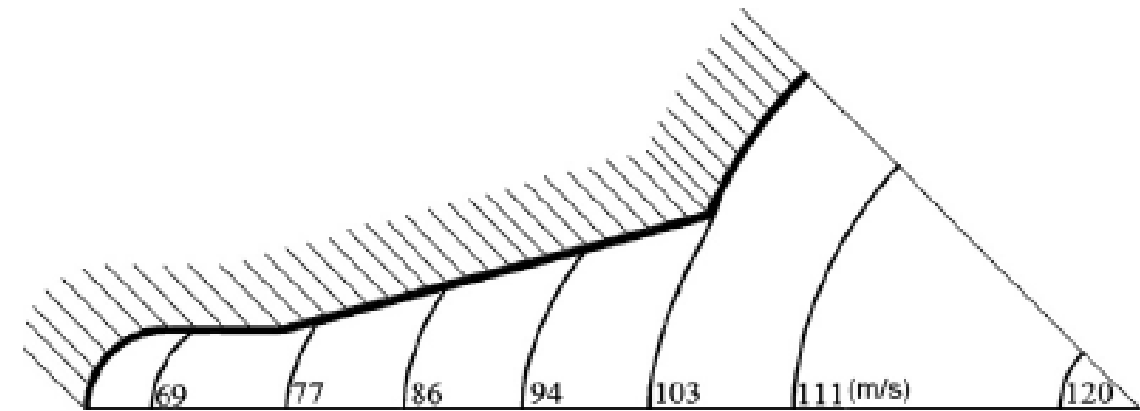


Fig. 6. The cross section of the propellant showing that at this section 1.91 m from the head end, the port is of finocyl geometry close to the nozzle end.

After much analysis, finally

If it can be taken that erosive burning is dominant over small regions for the early part of the combustion process as it happens in practice, *a simpler procedure can indeed be evolved*. In this approach, it is taken that an average heat flux is assumed prevalent over the entire burning perimeter. The more appropriate characteristic dimension to choose for evaluating the size effect through Re_0 is defined in terms of perimeter as P/π instead of $4A_p/P$. This will translate to d_p for circular port cross section as is needed. Calculations have been made for the above geometry dominated by erosive burning. The results are presented below. The data for grain–1 are set out in [Table 3](#).

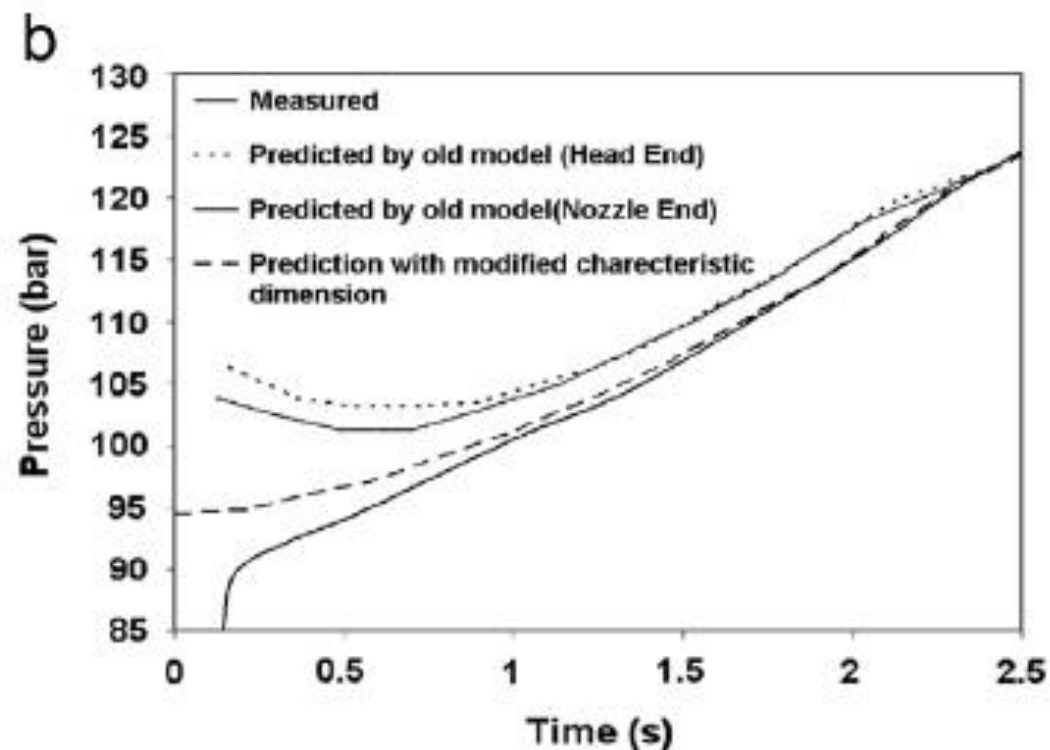
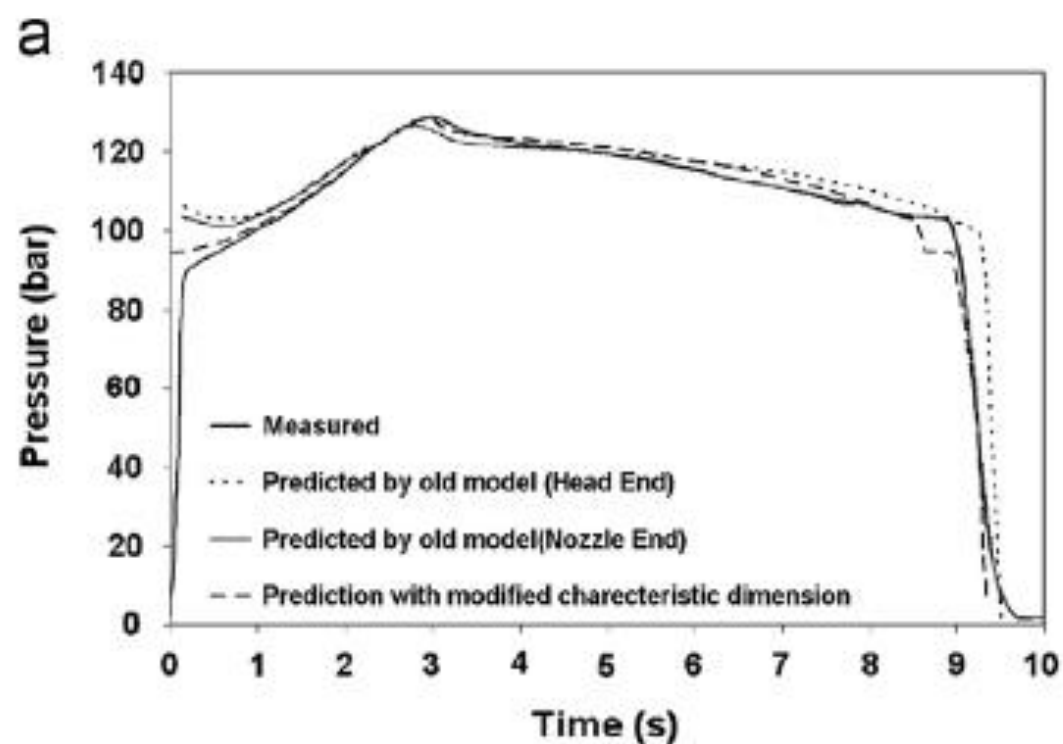


Fig. 9. Predicted and measured chamber pressures (a) full burn time (b) zoomed view to show the effect of modified model (Motor-1).

Table 3

Geometric and flow properties along the motor length ($p_c = 70$ atm, $T_c = 2800$ K, $L_p = \text{characteristic length} = \text{perimeter}/\pi$, $d_h = \text{hydraulic diameter}$).

x m	A_p cm ²	L_p m	\dot{m} kg/s	ρ_g kg/m ³	$G/\rho_p r_0$	$Re_r \times 10^4$	$g(L_p)$	η	$g(d_h)$	η'
0.44	35.6	0.067	1.01	7.68	21.8	1.46	15.6	1.0	15.6	1.0
0.88	35.9	0.067	1.98	7.64	42.3	1.46	30.3	1.0	30.3	1.0
1.43	53.3	0.112	3.3	7.58	47.5	2.44	31.9	1.0	34.5	1.0
1.73	78.8	0.173	4.9	7.55	47.7	3.75	30.3	1.0	34.8	1.0
1.91	79.7	0.174	6.01	7.52	57.9	3.79	36.8	1.01	42.2	1.06
2.08	80.4	0.176	7.47	7.50	71.3	3.81	45.2	1.09	52.0	1.14

This modification is what is now in the codes of propulsion system design at DRDO

One would imagine that the story has ended...all well.
Indeed not!

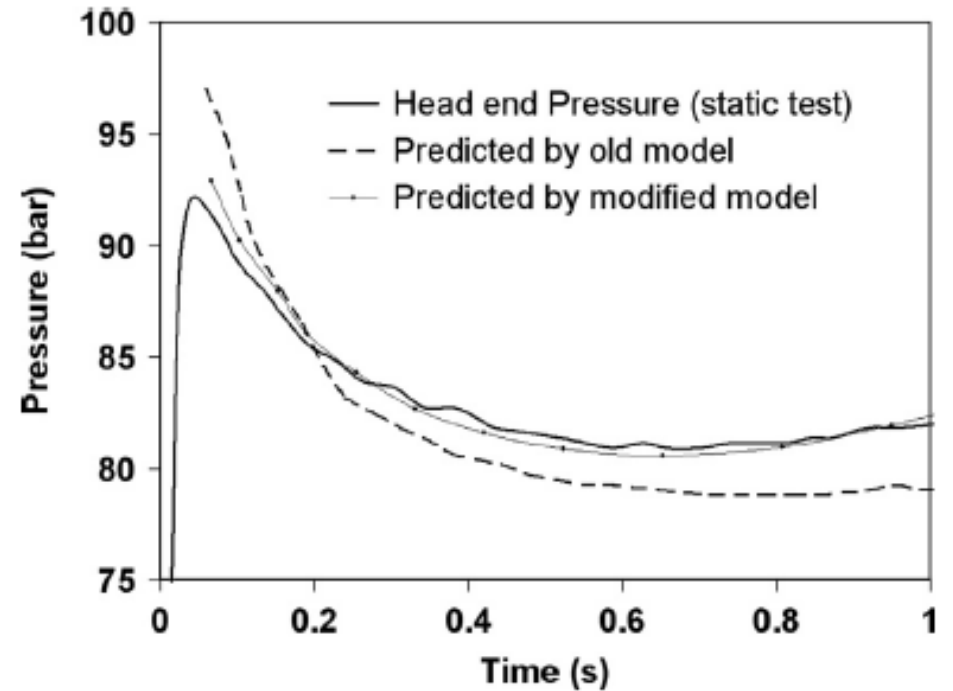


Fig. 10. Zoomed view of measured and predicted chamber pressures using the old and modified versions of the erosive burning model (Motor-2).

In 2006, appeared a paper in JPP:

JOURNAL OF PROPULSION AND POWER
Vol. 22, No. 5, September-October 2006

Erosive Burning of Aluminized Composite Propellants: X-Ray Absorption Measurement, Correlation, and Application

Hiroshi Hasegawa^{*}

NOF Corporation, Taketoyo, Aichi 470-2398, Japan

Masahisa Hanzawa[†]

Tokai University, Hiratsuka, Kanagawa 259-1292, Japan

and

Shin-ichiro Tokudome[‡] and Masahiro Kohno[§]

Japan Aerospace Exploration Agency, Sagamihara, Kanagawa 229-8510, Japan

DOI: 10.2514/1.7950

The erosive burning effects in a small test motor loaded with highly aluminized practical composite propellants have been investigated in detail by using x-ray absorption diagnostics to measure the propellant local regression. The motor was specially designed to have two propellant slabs and was called a double-slab motor. Significant erosive burning was found in the motor for several combustion pressure levels and ranges of mass flux in the port. The x-ray diagnostic system enabled observation of the time-wise change in the distribution of burning propellant surface during motor operation. A modified Dickinson-type simple correlative equation, which includes the effects of mass flux, mass burning rate, combustion pressure, and motor scale, was derived from the results of DSM firing tests. Parameters of the correlative equation were finally determined by taking into account the experimental results of both cylindrical test motors and practical full-scale motors.

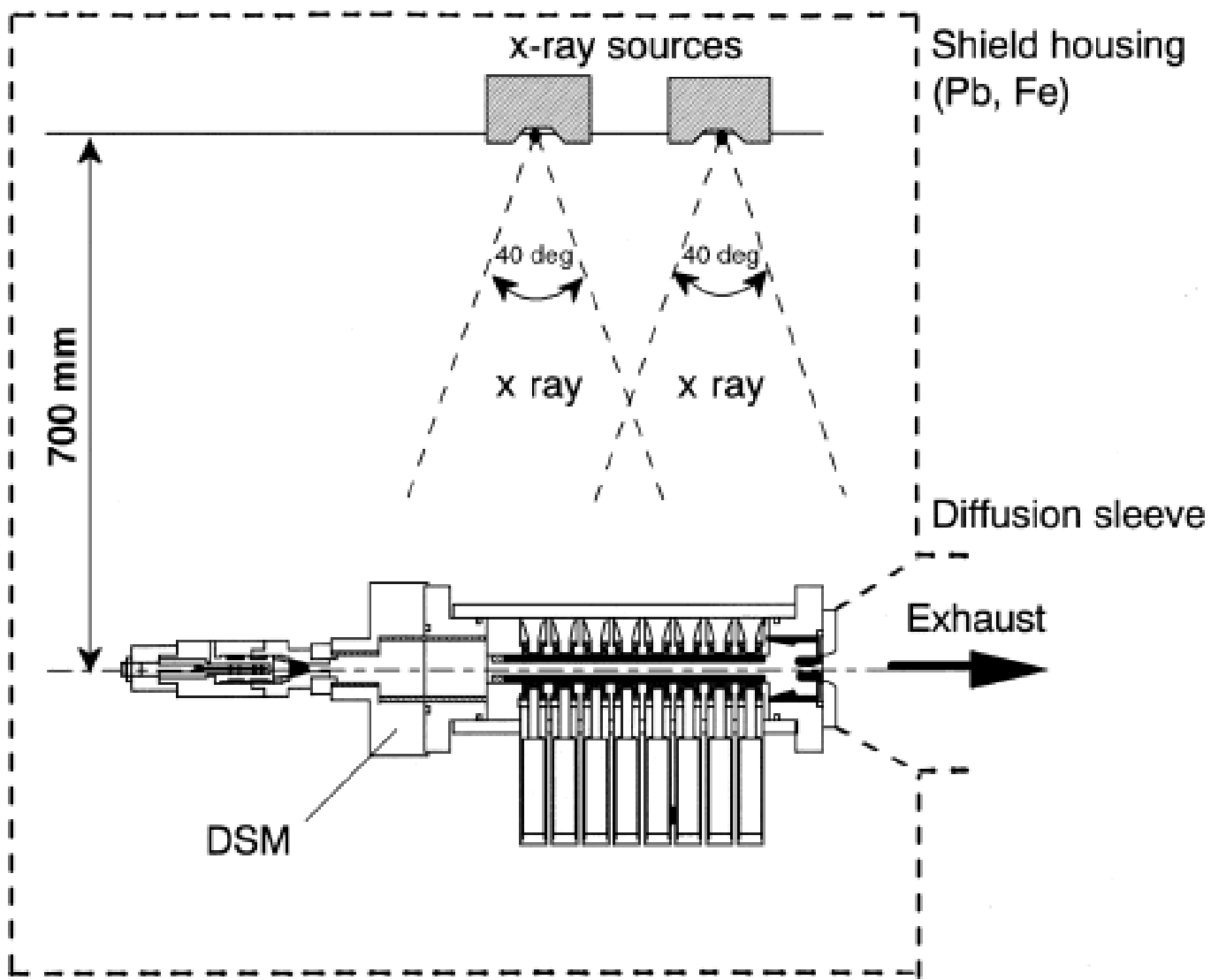


Fig. 2 Schematic of experimental setup.

For analyzing the erosive burning characteristics, the pressure curves and burning surface regression contours obtained in a series of DSM experiments are compared with calculations. For this purpose, a suitable correlative equation of erosive burning is needed. Many correlative equations have been proposed so far and are reviewed in [1,2]. Recently, Mukunda and Paul [12] proposed a new equation that was derived from empirical knowledge and theories of fluid dynamics. The authors have also studied theoretically erosive burning to develop a correlative equation for practical use [13,14]. However, any satisfactory correlative equation, which is appropriate enough from the view points of both theory and experiment, has not been obtained due to the complexities of port flow and combustion mechanisms in real motors. Therefore, Dickinson's correlation is employed in this study due to its simplicity and practicality. The original Dickinson's correlation is expressed as follows [11].

$$\frac{r}{r_0} = 1 + K_d G \left(1 - \frac{G_{cr}}{G} \right) \quad (4)$$

The correlations were....

And when this was inadequate, they adopted

$$\frac{r}{r_0} = \begin{cases} 1 + K_1 D_p^{-0.2} \left[G \left(1 - \frac{\hat{G}_{cr}}{\hat{G}} \right) \right]^\gamma & ; \hat{G} > \hat{G}_{cr} \\ 1 & ; \hat{G} \leq \hat{G}_{cr} \end{cases} \quad \hat{G}_{cr} = 10$$

And when that was inadequate for some motors, they adopted constants

$$K_1 = K_2 P^{-0.7}$$

$$K_2 = \begin{cases} 1.02 \times 10^{-3} & ; \text{Propellant No. 1} \\ 2.47 \times 10^{-4} & ; \text{Propellant No. 2} \end{cases}, [\text{m}^{2.2} \text{s MPa}^{0.7} / \text{kg}]$$

$$\gamma = 1.0$$

And further for some other motors

$$\gamma = 1.2,$$

$$K_2 = \begin{cases} 3.4 \times 10^{-4} & ; \text{propellant No. 1} \\ 7.0 \times 10^{-5} & ; \text{propellant No. 2} \end{cases}, [\text{m}^{2.6} \text{s}^{1.2} \text{MPa}^{0.7} / \text{kg}^{1.2}]$$

From Mallesh, ME Thesis, Aerospace Engg, IISc, 2014

- Dimensionless universal correlation for erosive burning was established more than a decade back and is used as a standard design tool for highly loaded tactical rocket motors.
- A number of cases of double slab and cylindrical motors are subject to analysis. Several features of inadequate ignition process that were being attributed to and coupled with erosive burning are addressed in this study.
- The comparison indicates that the predictions using the dimensionless correlation (due to hsm and pjp) are at least as good as their claims.
- This study therefore restores the adequacy (and perhaps necessity) of dimensionless approach that was sought to be disbanded by the Japanese workers.
- *What is disheartening to note is: Journal of Propulsion and Power has published an article in which there is an idea of claiming that dimensional correlations are more appropriate than dimensionless ones - Completely reversing scientific progress!*

The story is not completely over, yet!

An Approach to Analyse Erosive Characteristics of Two-Channel Combustion Chambers

Yanjie Ma, Futing Bao, Weihua Hui, Yang Liu and Ran Wei

Science and Technology on Combustion, Internal Flow and Thermo-Structure Laboratory,
Northwestern Polytechnical University, Xi'an, Shaanxi 710072, China

Correspondence should be addressed to Weihua Hui; zhongyuancao@163.com

In 2018, this paper was received for review:

1. Their concentration is L & R correlation - as to how they can find the constants that fit their experimental data of two-channel combustion system. Of course they did not cite our work! - a common experience generally from the West, but in this case also from China!!
2. After it was pointed out that gas dynamics can be combined with new universal law, they modified their manuscript - not fully appropriately though..... **I think the story will never end**

.....my end!